Journal of Alloys and Compounds 766 (2018) 291–296

Contents lists available at ScienceDirect

Journal of Alloys and Compounds

journal homepage: http://www.elsevier.com/locate/jalcom

Role of Ce substitution in the magneto-crystalline anisotropy of tetragonal $ZrFe_{10}Si_2$

D. Salazar [a, *], A. Martín-Cid [a], J.S. Garitaonandia [a, b], T.C. Hansen [c], J.M. Barandiaran [a, b], G.C. Hadjipanayis [d]

[a] BCMaterials, Basque Centre for Materials, Applications and Nanostructures, UPV/EHU Science Park, 48940 Leioa, Spain
[b] Faculty of Science and Technology, Univ. Basque Country (UPV/EHU), E-48080, Bilbao, Spain
[c] Institut Laue-Langevin, 71, Avenue des Martyrs, 38042, Grenoble, France
[d] Dept. Physics & Astronomy, University of Delaware, Newark, DE, 19716, USA

ARTICLE INFO

Article history:
Received 1 February 2018
Received in revised form
22 May 2018
Accepted 19 June 2018
Available online 20 June 2018

Keywords:
$ThMn_{12}$-type structures
Magnetocrystalline anisotropy
Rare-earth-free magnets

ABSTRACT

We report the study of $Zr_{1-x}Ce_xFe_{10}Si_2$ ($x = 0.0$, 0.3 and 0.6) compounds, with tetragonal $ThMn_{12}$ structure, by means of neutron diffraction and Mössbauer spectroscopy to understand the role of Ce in the increasing magneto-crystalline anisotropy. Fitting of the ^{57}Fe Mössbauer spectra to the three Fe atomic positions, namely 8i, 8j and 8f, indicate that Ce displaces Fe from the 8i to the 8j positions and in parallel increases the quadrupole splitting (QS) in position 8f, correlating with the increase of the magneto-crystalline anisotropy. However, the hyperfine field B_{hf} remains constant for all Ce substitutions. The full occupancy of the 8j positions by Fe at $Ce = 0.6$ can explain the instability of the $ThMn_{12}$ structure for similar and higher Ce concentrations. Neutron diffraction experiments show the evolution of the magnetic moment and crystal structure as a function of temperature, showing Ce to cause an increase of the lattice parameters and tetragonal distortion. A large anomaly of the expansion coefficient, due to the spontaneous magnetostriction, is also disclosed. These results support a pure geometric influence of Ce on the magneto-crystalline anisotropy through a selective distortion of the lattice.

1. Introduction

The critical and strategic character of rare earth (RE) elements as raw materials [1] has motivated an increased interest in the search for new rare-earth-lean and rare-earth-free hard magnetic materials for permanent magnets, with a performance not necessarily better than $Nd_2Fe_{14}B$, but also sufficient to fill the gap between ferrite and Nd-Fe-B magnets [2]. Tetragonal $R(Fe,M)_{12}$ compounds, with the $ThMn_{12}$ structure (1:12 for short), where R stands for rare earth and M is a transition metal or s-p element stabilizing the structure, are already rare-earth-lean and some of them present room-temperature ferromagnetism and a large uniaxial magneto-crystalline anisotropy [3]. Among them, special attention has been paid to those with cerium, the most abundant and least critical rare earth [4–8]. Zhou et al. [5] reported an unexpectedly high Curie temperature T_c of the $CeFe_{10}Si_2$ compound with the 1:12 structure, despite the unfavorable effect of the mixed-valence state of the Ce atoms on the T_c of the Ce-Fe compounds. Furthermore, in a recent work, it was found that the 1:12 structure is easily obtained in the $(Zr_{1-x}Ce_x)_{1.1}Fe_{10}Si_2$ alloys, with $0 \leq x \leq 0.6$, while for $x > 0.6$ a pure 1:12 phase is no longer stable and a secondary phase, with hexagonal Th_2Ni_{17}-type structure appears [9]. The rare-earth-free alloy $ZrFe_{10}Si_2$ shows a relatively high saturation polarization ($J_S = \mu_0 M_S \approx 1.1$ T) but a rather modest anisotropy constant ($K_1 = 0.74$ MJ m^{-3}), not enough for high-energy permanent magnets but superior to barium ferrites. $Zr_{0.4}Ce_{0.6}Fe_{10}Si_2$, however, presents the same magnetization, a K_1 value of 1.03 MJ m^{-3}, a Curie temperature in excess of 300 °C and a magnetic hardness parameter of 1.05 [9], meeting the requirements for high-energy permanent magnets proposed in Ref. [10]. The role of Ce on the structure and magneto-crystalline anisotropy of these compounds is worth analyzing, as it can give hints for other possible 1:12, RE lean/free compounds with increased anisotropy.

In this work, we study the effect of Ce substitution in $(Zr_{1-x}Ce_x)_{1.1}Fe_{10}Si_2$ ($x = 0.0$, 0.3 and 0.6) on the magneto-crystalline

* Corresponding author.
E-mail address: daniel.salazar@bcmaterials.net (D. Salazar).

https://doi.org/10.1016/j.jallcom.2018.06.225

anisotropy, through its influence on the crystalline and magnetic structure, determined by means of two nuclear techniques, ^{57}Fe Mössbauer spectroscopy (MS) and neutron powder diffraction (NPD), which are correlated with the magnetic properties.

2. Experimental

Alloys with nominal compositions of $(Zr_{1-x}Ce_x)_{1.1}Fe_{10}Si_2$ (x = 0.0, 0.3 and 0.6) were obtained by arc-melting 99.99% pure components. The alloys were heat-treated at 1000 °C during 24 h under vacuum in order to homogenize their composition and crystalline structure. Samples for magnetic measurements, neutron powder diffraction and Mössbauer spectroscopy were hand-milled in an agate mortar. The magnetic properties were measured with a vibrating sample magnetometer EZ7-VSM from MicroSense. Hysteresis loops of oriented powders were recorded at room temperature with a maximum magnetic field of 1.8 T. X-ray diffraction patterns were obtained using a Cu K_α radiation. NPD was performed in the D20 high-intensity two-axis diffractometer sited in the reactor of the Institute Laue Langevin in Grenoble. Experiments were performed with λ = 2.41 Å and 2θ ranging from 0° to 150.75° with a step size of 0.05°, between room temperature and 850 K. MS was performed at room temperature in the transmission geometry using a conventional constant-acceleration spectrometer with a ^{57}Co-Rh source. The MS results were analyzed by a least square method with the NORMOS program [11].

3. Results and discussion

3.1. Effect of Ce substitution on the crystalline and magnetic structure at room temperature

Magnetic properties of oriented fine powders were determined at room temperature (RT) to obtain the anisotropy field of the alloys. The orientation of the powders, as determined by preliminary X-ray diffraction, indicates the *c* axis as the easy axis. Initial magnetization curves parallel (∥) and perpendicular (⊥) to the orientation of the powders are shown in Fig. 1a. Saturation magnetization (M_s), obtained by the *law of approach to saturation* from the $M(H)_{\parallel}$ curves, is the same for all compositions (~120 A m^2 kg^{-1}) whilst Ce increases the anisotropy field from 2.03 T for x = 0 up to 2.5 T for x = 0.6. K_1 and K_2 anisotropy constants are determined from the initial magnetization curves perpendicular to the easy axis by the equation: $HM_s = 2K_1\left(\frac{M}{M_s}\right) + 4K_2\left(\frac{M}{M_s}\right)$, where *M* is the magnetization at *H* applied field. Values of K_1 are quite similar for all compounds (0.51 ± 0.02 MJ m^{-3}) whilst K_2 increases monotonously, being 0.24, 0.38 and 0.42 MJ m^{-3} for x = 0.0, 0.3 and 0.6, respectively. XRD patterns obtained in isotropic samples at RT are presented in Fig. 1b. They correspond to the pure 1:12 tetragonal phase with space group (I 4/m m m). The distortion of the crystal lattice induced by Ce results into an expansion of the lattice parameters. Table 1 summarizes the magnetic and structural properties.

It can be seen that the *a*-axis expansion due to Ce (≈1%) is exactly twice that of the *c*-axis, resulting in an overall increase of the tetragonal distortion (*a*/*c* ratio) of about 0.5%. This may be at the origin of the 25% increase of the magneto-crystalline anisotropy, as shown in Table 1.

It is well known that the stabilization of the $ThMn_{12}$-type structure in Fe rich phases requires the addition of a third element [3]. Elements like Mo or Ti substitute Fe atoms located exclusively in 8i position, resulting in a reduced number of different chemical neighbourhoods for the Fe positions [3] and the (spectral) contribution corresponding to each Fe crystallographic position split in a set of spectra to account for such different chemical neighbourhoods. In our case, Si atoms substitute Fe atoms at all positions, giving a large quantity of different Fe chemical neighbourhoods, which cannot be resolved in practice. Fig. 2, however, shows that Si atoms do not induce large changes in the hyperfine field values, and the Mössbauer spectra corresponding to each crystallographic Fe position can be properly described by a single but wider sextet, which simplifies the fitting. Results of the fitting are summarized in Table 2.

For an optimum fitting of the MS a paramagnetic component has been considered. This contribution is always below 2%, and the hyperfine parameters are different for each compound. Due to the extremely low amount of paramagnetic phase, hyperfine parameters are only a rough estimation, but still they can be assigned to traces of cubic $Zr_6Fe_{16}Si_7$ structure, which has been observed to coexist with $(Zr_{1-x}Ce_x)_{1.1}Fe_{10}Si_2$ when x = 0.0, or assigned to the $CeFe_2Si_2$ when x = 0.6, which is also a paramagnetic phase at RT

Table 1
Summary of magnetic and structural parameters of $(Zr_{1-x}Ce_x)_{1.1}Fe_{10}Si_2$ at RT: M_s: saturation magnetization, H_a: anisotropy field, a,c: lattice parameters.

Ce content	M_s (A·m^2 kg^{-1})	$\mu_0 H_a$ (T)	*a* (Å)	*c* (Å)	*a*/*c*
x = 0.0	120	2.03	8.274	4.701	1.760
x = 0.3	120	2.31	8.303	4.707	1.764
x = 0.6	120	2.50	8.354	4.724	1.768

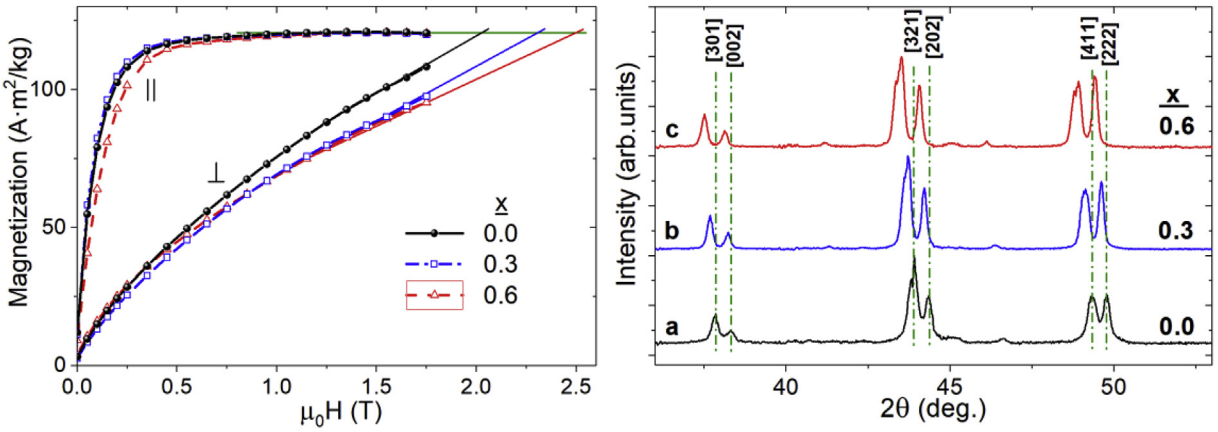

Fig. 1. a) RT isotherms for field-oriented powders in parallel (∥) and perpendicular (⊥) directions to the easy axis of magnetization and **b)** XRD at RT for (a) $Zr_{1.1}Fe_{10}Si_2$, (b) $(Zr_{0.7}Ce_{0.3})_{1.1}Fe_{10}Si_2$ and (c) $(Zr_{0.4}Ce_{0.6})_{1.1}Fe_{10}Si_2$ samples.

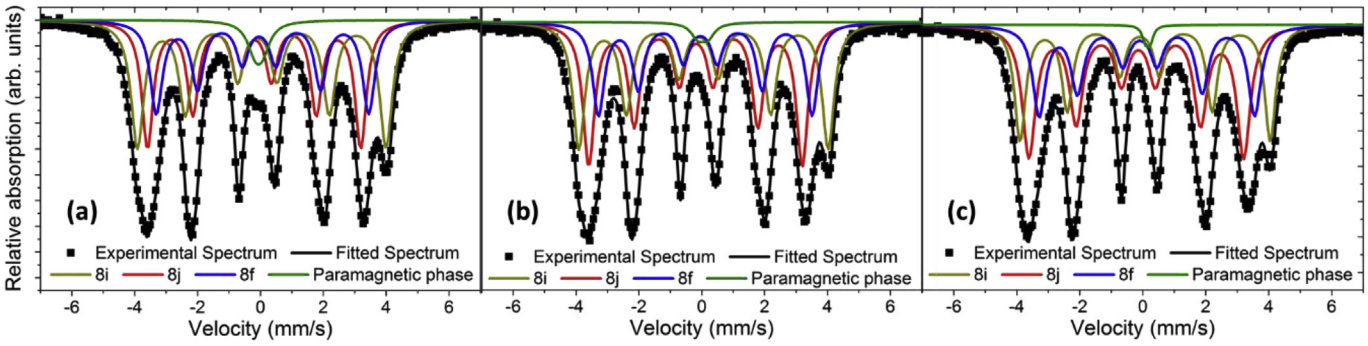

Fig. 2. Mössbauer spectra at RT for (a) $Zr_{1.1}Fe_{10}Si_2$, (b) $(Zr_{0.7}Ce_{0.3})_{1.1}Fe_{10}Si_2$ and (c) $(Zr_{0.4}Ce_{0.6})_{1.1}Fe_{10}Si_2$ samples.

Table 2
Mössbauer hyperfine parameters for $(Zr_{1-x}Ce_x)_{1.1}Fe_{10}Si_2$ compounds. ISO = Isomer Shift, QS = Quadrupole Splitting, B_{hf} = hyperfine field, WID = line width. The Fe content is referred only to the 1:12 phase, so the total Fe in 8i, 8j and 8f positions add to 100% to make clear the preferential occupancies of Fe and Si. Natural Width of the line is ≈ 0.27 mm/s. Values in bold are referred in the text below.

Ce content	Fe position	% Fe	ISO (mm/s)	QS (mm/s)	B_{hf} (T)	WID (mm/s)
x = 0.0	8i	**38**	0.07	0.14	24.5	0.44
	8j	**35**	−0.09	−0.01	21.0	0.44
	8f	27	0.11	**0.11**	21.0	0.47
	Paramagnetic	<2	0.03	0.21	–	0.32
x = 0.3	8i	**35**	0.08	0.16	24.6	0.46
	8j	**39**	−0.09	−0.02	21.1	0.45
	8f	26	0.13	**0.16**	21.1	0.45
	Paramagnetic	<1	0.20	0.20	–	0.27
x = 0.6	8i	**32**	0.09	0.17	24.6	0.42
	8j	**40**[a]	−0.07	−0.06	21.1	0.52
	8f	28	0.12	**0.23**	21.2	0.49
	Paramagnetic	<1	0.40	0.17	–	0.27

[a] 40% Fe means all available 8j sites are already occupied by Fe.

[9,12]. A minimum amount of such phases were also detected in our NPD patterns (see Fig. 3b).

Note that the maximum Fe occupancy at any crystallographic site of the 1:12 structure is 4 atoms, i.e. 40% of the 10 Fe atoms per formula unit. Table 2 shows that the preferred Si occupancy is the 8f site for all samples, but for x = 0 there is also Si in the other two positions. Ce progressively displaces Fe from the 8i to the 8j positions, so Si is in turn displaced from the 8j to 8i sites. For x = 0.6, there is no Si in 8j position. Such preferential atomic occupancy has an influence on the magneto-crystalline anisotropy, as confirmed by the increase of the quadrupole splitting (QS) in position 8f. Moreover, the tendency of Ce to displace Fe to the 8j position can lead to instability of the 1:12 phase since, although the displacement of Fe from 8i is linear, it is not linear for 8j, leading to a formation of a secondary phase when x is slightly below 0.6. Once such positions are fully occupied a further increase of Ce cannot be accommodated by the same crystal structure, because no more Fe can be displaced to the 8j position.

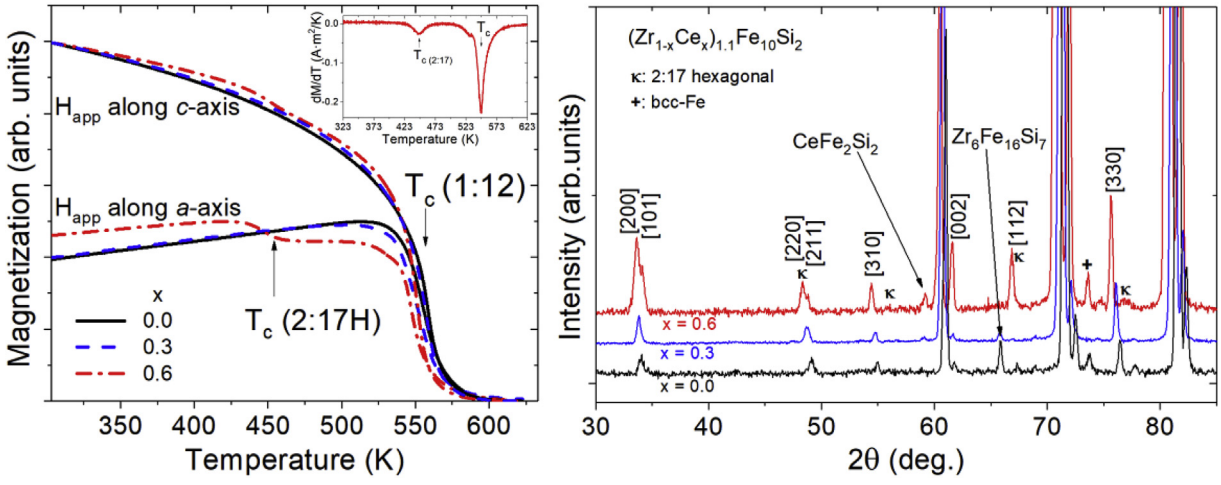

Fig. 3. a) M(T) curves for all oriented samples with the magnetic field (10 mT) applied along the a- and c-axis. b) Magnified NPD patterns for all samples at RT.

3.2. Temperature evolution of the magnetic and structural properties

Once the effect of Ce-substitution on the room temperature structural and magnetic properties was analyzed, a detailed study of their properties as a function of temperature was carried out. Measurements of magnetization as a function of temperature were performed on oriented samples (Fig. 3a), with the field applied along the easy axis (*c*) and the hard axis (*a*) of magnetization. Fig. 3a shows clear differences on M(T) depending on the field orientation for all samples. In particular for x = 0.6, and only for this composition, when the field is applied along the *a*-axis (dash dot line) the magnetization shows two transitions; the first one around 450 K could be associated with a possible secondary magnetic phase at this temperature. The second transition is the Curie point of the 1:12 tetragonal phase (~560 K). The transition at 450 K was not clearly evidenced when the field was applied along the *c*-axis. We can explain this behavior in terms of a small amount of a secondary magnetic phase, probably a 2:17 hexagonal phase, which has been reported to appear for x > 0.6 [9], and having $T_c \sim 473$ K. Some of the 2:17 phase diffraction peaks can be distinguished in the NPD pattern (Fig. 3b). This phase could be hidden in the MS since its contribution is small and, once distributed into several sextets, can be blurred in the background noise. However, the WID for the 8j position for x = 0.6 is larger (0.52 mm/s) than in the others, hinting for an extra ferromagnetic contribution at RT in this compound.

NPD patterns at temperatures between 300 and 850 K were recorded for all samples. The diffraction pattern for the sample $(Zr_{0.7}Ce_{0.3})_{1.1}Fe_{10}Si_2$ in the ferromagnetic (320 K) and paramagnetic state (650 K) is shown in Fig. 4. It presents the $ThMn_{12}$-type tetragonal structure at both temperatures. By subtracting the ferromagnetic and paramagnetic patterns, magnetic contributions are observed for [110] and [220] diffraction peaks, which indicates that the magnetic moment lies along the direction perpendicular to these diffraction planes, i.e., along the *c* axis. Although the insufficient magnetic contribution to the diffraction makes the extraction of magnetic moments unreliable, the magnetic intensity decreases monotonously up to T_c, and therefore the easy direction is unchanged in all the temperature range.

The evolution the intensity and position of [301] and [002] diffraction peaks, which are related with the *a*- and *c*-lattice parameters respectively, are shown in Fig. 5a. Both peaks show different trends. The [301] peak shifts linearly with temperature, while the [002] displacement is more complex. To study the expansion of the lattice parameters with temperature, NPD patterns were fitted using the Fullprof suite in sequential mode. Results for *a*- and *c*-lattice parameters are shown in Fig. 5b and c, respectively, for all samples. In agreement with Fig. 5a, *a* shows a continuous increase with increasing temperature; *c*, however, keeps almost constant when the temperature is below 550 K. For higher temperatures, *c* starts to increase following a linear trend. The change in the *c*-lattice parameter occurs at the Curie point of our samples.

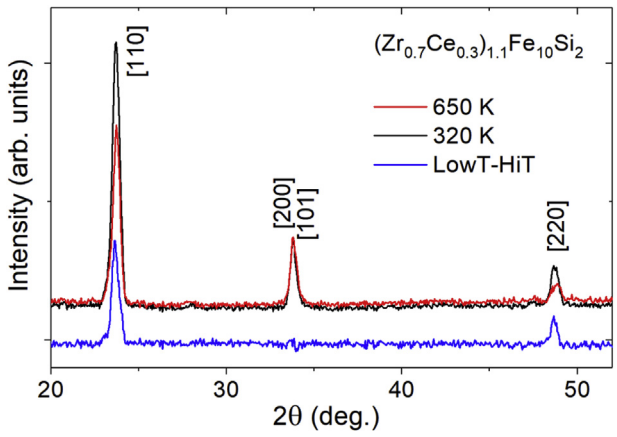

Fig. 4. Neutron powder diffraction for x = 0.3, at the ferromagnetic (320 K) and the paramagnetic state (650 K). The difference show the magnetic peaks are only [110] and [220].

Linear thermal expansion coefficients (α_L) were estimated from high temperature data, in the paramagnetic state (above 600 K). Extrapolated to RT, α_L along the *a*-axis are 1.69×10^{-5}, 1.45×10^{-5} and 1.48×10^{-5} K^{-1} for x = 0.0, 0.3 and 0.6 respectively, and along *c*-axis 0.98×10^{-5}, 1.00×10^{-5} and 1.00×10^{-5} K^{-1}. Although the α_L values are quite similar for different compositions, they depend considerably on the crystalline orientation, being around a 50% higher along the *a*-than along the *c*-axis. These values are close to those reported in similar systems $(Y(Fe,Mo)_{12})$ [13] which show a mainly linear thermal expansion.

Extrapolating the linear behavior of *c* at high temperatures below T_c (solid line in Fig. 5c), we can obtain the difference on the c lattice parameter (Δc) due to the anomaly. These differences are represented in Fig. 6 and follow a clear M^3 law.

The *c*-axis lattice anomaly is clearly a magnetic one, as appears only below T_c. It is directed along the magnetic moment direction and, hence, can be assigned to a large positive spontaneous magnetostriction of $\lambda = \Delta c/c \approx 1500$ ppm at RT. This is of the same order of magnitude of the (Tb-Dy)Fe_2 (TERFENOL-D) with $\lambda \approx 2000$ ppm at RT, the highest magnetostrictive compound known to date [14,15].

The direct dependence of Δc vs. $(M_s)^3$ (Fig. 6) indicates a pure single ion contribution to the magnetostriction, indicating also the same origin for the uniaxial anisotropy, for all the compounds. Such analysis of the thermal dependence of the magnetostriction was proposed by O'Handley [16,17] in the 80's and successfully used for studying magnetostriction in amorphous ferromagnets [18]. The single ion term is due to the interaction between the Fe electron orbitals and the crystal electric field and scales as M^3, while a possible two ions contribution, which could arise from anisotropic exchange between different magnetic atoms, like Fe and Ce, will follow a M^2 law [16].

4. Conclusions

In this study, we have found that the increase of magnetic anisotropy in $Zr_{1-x}Ce_xFe_{10}Si_2$ (from $\mu_0 H_a = 2.0$ T, for x = 0.0, up to 2.5 T for x = 0.6) correlates with the increase of the cell volume and the tetragonal distortion (*a*/*c*) of the lattice produced by the Ce substitution of Zr. However, no change in the magnetization is observed. Mossbauer spectroscopy has shown that Ce displaces Fe from the 8i to the 8j position in the 1:12 structure and increases the crystal electric field gradient in the 8f position of Fe, leaving the hyperfine field unchanged in all Fe positions. The complete filling of 8j positions by Fe, for x slightly below 0.6, leads to the instability of the 1:12 phase upon a further increase of Ce, as when x = 0.6, which cannot be accommodated by the same crystal structure, facilitating the formation of the 2:17 phase.

An analysis on the thermal expansion was also carried out observing a *c*-lattice anomaly below T_c, which is assigned to a giant magnetostriction of about 1500 ppm in all the compounds at RT. The M^3 dependence of the magnetostriction reveals a pure single ion (or crystal field) origin of both the magnetostriction and the anisotropy in these compounds. The results so far indicate a pure geometric origin of the magnetic anisotropy. Therefore, we can expect that any ion similar in size to Ce (as will be mischmetal for

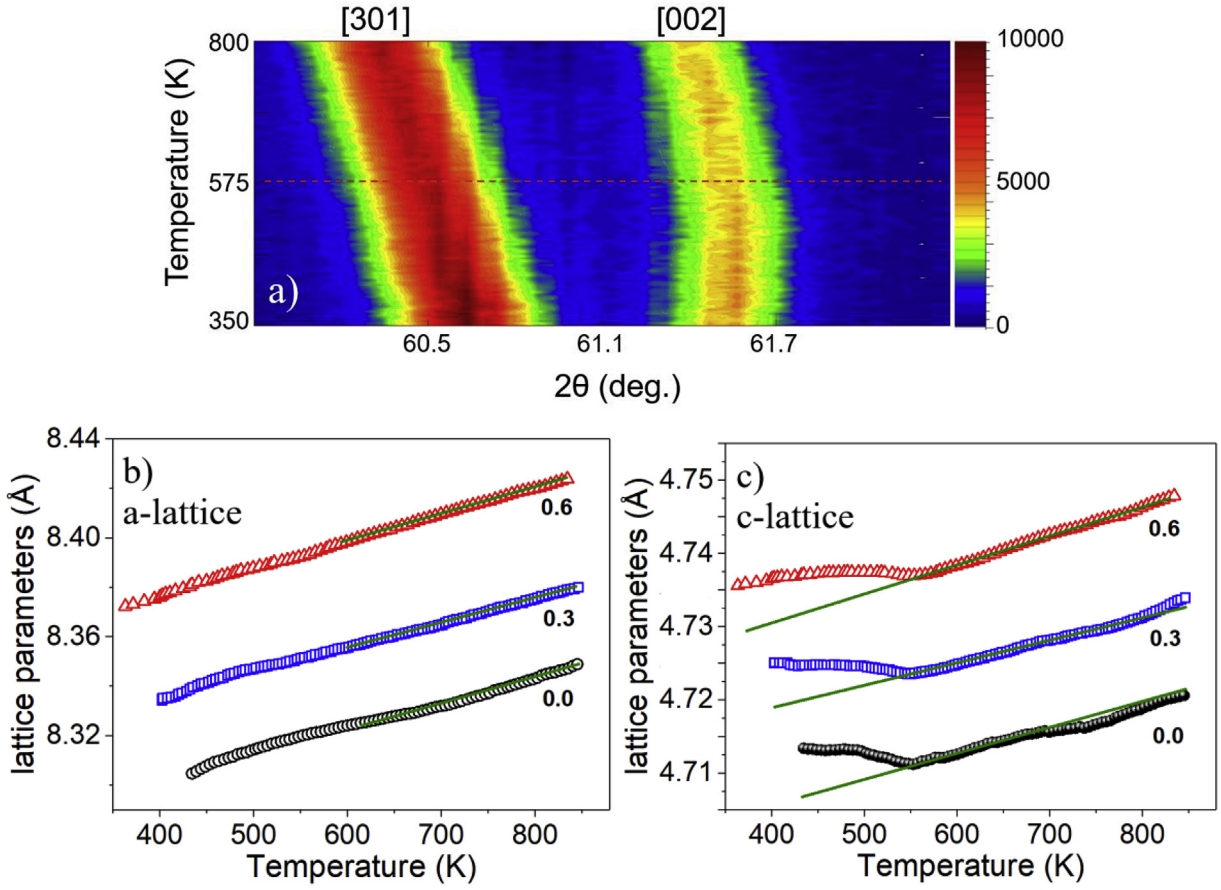

Fig. 5. a) Neutron powder thermodiffraction for the sample with x = 0.3. b) a- and c) c-lattice parameters as a function of temperature for all samples.

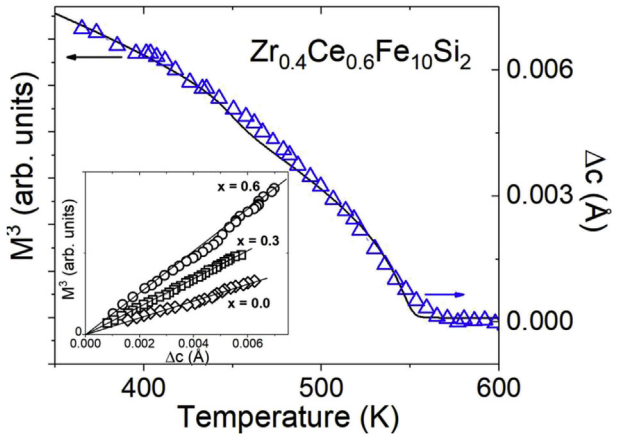

Fig. 6. Evolution of Δc for x = 0.6 as a function of temperature compared with the corresponding M^3(T) curve. The inset shows the M^3 dependence of Δc for all the alloys.

instance) can lead to the same increase in anisotropy of the pure $ZrFe_{10}Si_2$ compound.

Acknowledgments

Work has received funding from the DOE BES-DE-FG02-90ER45413 and European Union's Horizon 2020 research and innovation programme under grant agreement No 686056 (NOVAMAG).

References

[1] Tackling the Challenges in Commodity Markets and on Raw Materials, COM, 2011, p. 25.
[2] J.M.D. Coey, Permanent magnets: plugging the gap, Scr. Mater. 67 (2012) 524–529, https://doi.org/10.1016/j.scriptamat.2012.04.036.
[3] K.H.J. Buschow, Permanent magnet materials based on tetragonal rare earth compounds of the type $RFe_{12-x}M_x$, J. Magn. Magn. Mater. 100 (1991) 79–89, https://doi.org/10.1016/0304-8853(91)90813-P.
[4] D. Goll, R. Loeffler, R. Stein, U. Pflanz, S. Goeb, R. Karimi, G. Schneider, Temperature dependent magnetic properties and application potential of intermetallic Fe_{11-x} Co_x TiCe, Phys. Status Solidi Rapid Res. Lett. 8 (2014) 862–865, https://doi.org/10.1002/pssr.201409270.
[5] C. Zhou, F.E. Pinkerton, J.F. Herbst, High Curie temperature of Ce–Fe–Si compounds with $ThMn_{12}$ structure, Scr. Mater. 95 (2015) 66–69, https://doi.org/10.1016/j.scriptamat.2014.10.006.
[6] C. Zhou, K. Sun, F.E. Pinkerton, M.J. Kramer, Magnetic hardening of Ce_{1+x} Fe $_{11-y}$ Co_y Ti with $ThMn_{12}$ structure by melt spinning, J. Appl. Phys. 117 (2015) 17A741, https://doi.org/10.1063/1.4918562.
[7] A.M. Gabay, A. Martín-Cid, J.M. Barandiaran, D. Salazar, G.C. Hadjipanayis, Low-cost $Ce_{1-x}Sm_x$ (Fe, Co, Ti)$_{12}$ alloys for permanent magnets, AIP Adv. 6 (2016) 56015, https://doi.org/10.1063/1.4944066.
[8] A. Martin-Cid, D. Salazar, A.M. Schönhöbel, J.S. Garitaonandia, J.M. Barandiaran, G.C. Hadjipanayis, Magnetic properties and phase stability of tetragonal $Ce_{1-x}Sm_xFe_9Co_2Ti$ 1:12 phase for permanent magnets, J. Alloys Compd. 749 (2018) 640–644, https://doi.org/10.1016/j.jallcom.2018.03.325.
[9] A.M. Gabay, G.C. Hadjipanayis, $ThMn_{12}$-type structure and uniaxial magnetic anisotropy in $ZrFe_{10}Si_2$ and $Zr_{1-x}Ce_xFe_{10}Si_2$ alloys, J. Alloys Compd. 657 (2016) 133–137, https://doi.org/10.1016/j.jallcom.2015.10.073.
[10] R. Skomski, J.M.D. Coey, Permanent Magnetism, Taylor & Francis, New York, 1999.
[11] R.A. Brand, J. Lauer, D.M. Herlach, The evaluation of hyperfine field distributions in overlapping and asymmetric Mossbauer spectra: a study of the amorphous alloy $Pd_{77.5-x}Cu_6Si_{16.5}Fe_x$, J. Phys. F Met. Phys. 13 (1983) 675–683, https://doi.org/10.1088/0305-4608/13/3/018.
[12] A.M. Gabay, R. Cabassi, S. Fabbrici, F. Albertini, G.C. Hadjipanayis, Structure and permanent magnet properties of $Zr_{1-x}R_xFe_{10}Si_2$ alloys with R = Y, La, Ce, Pr and Sm, J. Alloys Compd. 683 (2016) 271–275, https://doi.org/10.1016/

j.jallcom.2016.05.092.
[13] H. Sun, M. Akayama, K. Tatami, H. Fujii, Magnetic properties of $YFe_{12-x}Mo_x$ and $YFe_{12-x}Mo_xN_y$ ($0.5 \leq x \leq 4.0$, $y \approx 1$), Phys. B Condens. Matter. 183 (1993) 33–39, https://doi.org/10.1016/0921-4526(93)90050-G.
[14] A.E. Clark, E.P. Wolfhart, Ferromagnetic Materials, North Holland, Amsterdam, 1980.
[15] G. Engdahl, Handbook of Giant Magnetostrictive Materials, Academic Press, San Diego, CA, 2000.
[16] R.C. O'Handley, M.O. Sullivan, Magnetostriction of $Co_{80-x}T_xB_{20}$ (T = Fe, Mn, Cr, or V) glasses, J. Appl. Phys. 52 (1981) 1841–1843, https://doi.org/10.1063/1.329546.
[17] R.C. O'Handley, Magnetostriction of transition-metal-metalloid glasses: temperature dependence, Phys. Rev. B. 18 (1978) 930–938, https://doi.org/10.1103/PhysRevB.18.930.
[18] J.M. Barandiarán, A. Hernando, O.V. Nielsen, Temperature dependence of magnetostriction in $[Co_{1-x}(FeNi)_x]_{75}Si_{15}B_{10}$ amorphous alloys, J. Magn. Magn. Mater. 46 (1985) 317–320, https://doi.org/10.1016/0304-8853(85)90052-6.